

# A Geometric Approach to Trajectory Design for an Autonomous Underwater Vehicle: Surveying the Bulbous Bow of a Ship

R.N. Smith, *Member IEEE*, D. Cazzaro, L. Invernizzi, G. Marani S.K. Choi and  
M. Chyba

## Abstract

In this paper, we present a control strategy design technique for an autonomous underwater vehicle based on solutions to the motion planning problem derived from differential geometric methods. The motion planning problem is motivated by the practical application of surveying the hull of a ship for implications of harbor and port security. In recent years, engineers and researchers have been collaborating on automating ship hull inspections by employing autonomous vehicles. Despite the progresses made, human intervention is still necessary at this stage. To increase the functionality of these autonomous systems, we focus on developing model-based control strategies for the survey missions around challenging regions, such as the bulbous bow region of a ship. Recent advances in differential geometry have given rise to the field of geometric control theory. This has proven to be an effective framework for control strategy design for mechanical systems, and has recently been extended to applications for underwater vehicles. Advantages of geometric control theory include the exploitation of symmetries and nonlinearities inherent to the system.

Here, we examine the posed inspection problem from a path planning viewpoint, applying recently developed techniques from the field of differential geometric control theory to design the control

This research is supported in part by National Science Foundation grant DMS-0608583, and in part by Office of Naval Research grants N00014-03-1-0969, N00014-04-1-0751 and N00014-04-1-0751.

R.N. Smith: Computer Science Department, Robotic Embedded Systems Laboratory, 3710 S. M<sup>c</sup>Clintock Avenue, Ronald Tutor Hall (RTH 512), University of Southern California, Los Angeles, CA 90089

M. Chyba: Mathematics Department, College of Natural Sciences, University of Hawai‘i, Honolulu, HI 96822, USA

D. Cazzaro, L. Invernizzi: College of Engineering, Sant’Anna School of Advanced Studies, Pisa, Pi, 56127, Italy

G. Marani, S.K. Choi: Autonomous Systems Laboratory, College of Engineering, University of Hawai‘i, Honolulu, HI 96822, USA

strategies that steer the vehicle along the prescribed path. Three potential scenarios for surveying a ship's bulbous bow region are motivated for path planning applications. For each scenario, we compute the control strategy and implement it onto a test-bed vehicle. Experimental results are analyzed and compared with theoretical predictions.

### **Index Terms**

Bulbous Bow Survey, Autonomous Underwater Vehicle, Trajectory Design, Geometric Control Theory

## I. INTRODUCTION

Approximately 90% of the goods traded throughout the world are carried by the international shipping industry. With incentives of competitive freight costs during a time of increasing fuel expenses, seaborne trade continues to expand. Currently, there are more than 50,000 merchant ships trading internationally. This fleet belongs to more than 150 nations, and employs over one million seafarers. With a high volume of ships arriving from worldwide destinations, it is of utmost importance to monitor and protect the ports that facilitate each country's trading market. To this end, it has become an interest of border police and port authorities to examine the hulls of ships for potentially dangerous attachments, e.g., explosives, before they enter the harbor.

Currently, these tasks are performed by highly-skilled human divers. Such labor intensive work introduces fatigue and poses multiple potential risks to the divers. In particular, in the presence of hazardous elements these risks can be life-threatening. To reduce the risk to human life, the use of Remotely Operated Vehicles (ROVs) has become a useful alternative. However, this also requires intense human involvement to safely navigate the ROV around the ship. Moreover, the area around a ship in berth can be highly cluttered, and tethered vehicles can experience impediments in reaching confined due to tether entanglement and piloting error. Both of these methods cost time and money, and cannot guarantee full coverage.

In an effort to provide a more comprehensive and cost-effective solution to this problem, engineers have been working on automating this process by employing Autonomous Underwater Vehicles (AUVs). AUVs offer several advantages over the previously mentioned approaches; the risk to humans is eliminated, the capability to dive in cluttered environments is improved,

and being autonomous, they can provide around-the-clock surveillance of incoming ships and surrounding port facilities.

A pioneering and innovative approach to automating ship hull surveys is presented in [1]. Here, the authors demonstrate the use of a Doppler Velocity Logger (DVL) to allow the vehicle to lock onto a ship's hull and perform fixed-distance, hull-relative motions to complete a survey. This approach is shown to be highly-effective in inspecting the sides of the hull, i.e., flatter regions, however human intervention was required in the proximity of more complex regions, e.g., the bulbous bow, running gear, full longitudinal cross-section, etc. The reason for these issues is that the vehicle's trajectory is strictly dependant upon sensor input from the DVL. If the DVL loses lock on the ship's hull, the AUV loses localization, and thus is unable to complete the mission without intervention. This situation can result in areas where the curvature of the hull changes rapidly over a short distance, e.g., the bulbous bow. Additionally, a DVL is an instrument that consumes relatively large amounts of power. For an autonomous system, it is of interest to employ the use of such sensors on a limited basis to extend the deployment duration of the vehicle.

In an effort to increase the functionality of autonomous systems, such as that described in [1], we focus on developing control strategies for AUVs to survey these more challenging regions. In this paper, we consider the bulbous bow region of a ship. Many of the merchant vessels currently in operation have a bulbous bow similar to that seen in Fig. 1. The bulb is a protrusion from the front of the hull, positioned to sit just below the design water line. Hydrodynamically, the bulb serves the purpose of reducing the height of the bow wake of the vessel, thus decreasing hull drag



Fig. 1. USS George H.W. Bush (CVN 77), [2].

and achieving better efficiency. Bulbs come in all different shapes and sizes and are optimized for a given ship design. It is imperative to take added care in the inspection and maintenance of the bow, as the efficiency of the ship greatly depends on its effectiveness. Since the bulb is a protrusion, damage caused from ship-dock or ship-ship interaction is always a concern. Although the primary motivations of this study are safety and hazard mitigation, the bulbous

bow provides an interesting control theory problem for which to consider motion planning and trajectory design, due to its peculiar shape. To our knowledge, there is no previous research specifically dedicated to this topic.

We approach this problem from a path planning viewpoint, with the motivation to reduce the reliance on navigational instruments that tend to consume large amounts of energy. By utilizing a model-based path planning techniques to design trajectories and control strategies, and implementing them with the assistance of sensors and feedback controllers, we aim to provide a contribution towards a reliable system for autonomous hull inspection. The foundation upon which we build our path planning approach is that of differential geometric control theory. Previous research has shown that geometric control theory is a useful and effective way to design and compute control strategies for many simple mechanical control systems<sup>1</sup>, including the submerged rigid body (e.g., [3], [4]). Additionally, the rigid body submerged in an ideal fluid is used as a running example throughout [5], [6], [7] and [8]. This differential geometric architecture, and associated path planning techniques have been extended to include external forces, such as viscous damping and restoration forces resulting from buoyancy and gravity, in the series of publications [9], [10] and [11].

Supported by the research presented in the aforementioned references, differential geometry provides the framework and structure necessary to consider an agile AUV capable of moving in all six degrees-of-freedom (DOF). This *a priori* consideration of path planning can outweigh the computational cost of learning system parameters from a model-based control approach, and lower the need for accurate and energy consuming sensors. Additionally, this framework includes a straightforward method to accommodate under-actuated scenarios, such as thruster failure for a fully-actuated vehicle, or standard path planning for an under-actuated torpedo-shaped vehicle. A complete theoretical analysis of our proposed approach with experimental results has been thoroughly exposed in [11]. In this paper, we present the results of several experiments conducted on a test-bed AUV; the Omni-Directional Intelligent Navigator (ODIN), which is owned and maintained by the Autonomous Systems Laboratory, College of Engineering, University of Hawai'i.

<sup>1</sup>A simple mechanical control system is one that has a Lagrangian expressing the energy of the system as potential minus kinetic.

The control strategies presented in this study are implemented onto ODIN in full open loop to demonstrate the effectiveness of the geometric theory in designing implementable trajectories, and to assess the vehicle's performance in executing the trajectory without any interference from sensed data. In a real-world application, we understand that a feedback control loop would be implemented to track the computed path, as unknown external disturbances, e.g., currents, render open-loop controllers useless by themselves. However, developing model-based control strategies that exploit symmetries and nonlinearities within the dynamics of a vehicle, as the differential geometric techniques allow, could lead to an AUV relying less upon sensor input for navigation. In addition to trajectory design for test-bed vehicles, we are also interested in implementable closed-loop solutions for ocean-going AUVs. Preliminary work on robust feedback tracking of AUVs can be found in [12] and [13].

We continue our presentation in Section II by developing the equations of motion for a rigid body submerged in a viscous fluid in both the traditional manner as well as in the language of differential geometry. These geometric equations are not a new formulation of the standard equations, but simply a translation and slight abstraction into the differential geometric architecture. In Section II-A we provide the technical specifications and physical characteristics of ODIN, the test-bed vehicle used for our experiments. In Section III, we describe the trajectory method and the calculation of the control strategies. We additionally address the necessary technique to transform the calculated control strategies into implementable controls for ODIN. Three scenarios for surveying the bulbous bow are motivated and described in Section IV. For each scenario, we compute the desired control strategy, implement it onto ODIN, and compare the experimental results to our theoretical predictions. An overall assessment is included for the procedure and experiments conducted, with ideas and motivations for future research efforts.

## II. EQUATIONS OF MOTION

To model the equations of motion governing a rigid body, it is necessary to work with two coordinate reference frames; one inertial (Earth-fixed) and one for the vehicle (body-fixed). For low-speed marine vehicles, such as the one studied here, the Earth's movement has a negligible effect on the dynamics of the vehicle. Thus, the Earth-fixed frame may be considered as an inertial frame. The inertial reference frame  $\Sigma_I : (O_I, \{s_1, s_2, s_3\})$ , shown in Fig. 2, is a right-handed, orthogonal coordinate system defined with the  $s_1$  and  $s_2$  axes lying in the horizontal

plane perpendicular to the direction of gravity, while the  $s_3$  axis is orthogonal to the  $s_1 - s_2$  plane and taken to be positive in the direction of gravity. We also refer to the inertial reference frame as the spatial reference frame. Note that since we are considering an unbounded fluid domain, we are free to select an arbitrary position for the inertial frame, preferably in a location such that the depth of the vehicle is non-negative.

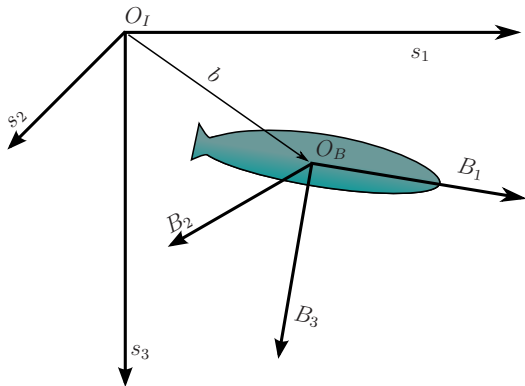


Fig. 2. Earth-fixed and body-fixed coordinate reference frames.

The body-fixed frame  $\Sigma_B : (O_B, \{B_1, B_2, B_3\})$ , shown in Fig. 2, is a right-handed, orthogonal reference frame defined with the origin  $O_B$  located at a chosen location, and the body axes  $B_1, B_2$  and  $B_3$  coinciding with the principle axes of inertia. The longitudinal ( $B_1$ ) and transverse ( $B_2$ ) axes are taken positive to the fore and starboard, respectively. The configuration of a rigid body in six DOF can be described using  $\boldsymbol{\eta} = (x, y, z, \phi, \theta, \psi)^t = (\mathbf{b}, \boldsymbol{\eta}_2)^t$ , where  $\boldsymbol{\eta}_2 = (\phi, \theta, \psi)^t$  is the orientation of the body, relative to the spatial frame, and  $\mathbf{b} = (x, y, z)^t$  is the body's relative position. A body's configuration  $\boldsymbol{\eta}$  can also be represented as an element of the Special Euclidean group  $SE(3)$ :  $(\mathbf{b}, R)$ , where  $R \in SO(3)$  is a rotation matrix describing the orientation of the body and  $SO(3)$  is the group of orthogonal matrices that have determinant equal to one. In the following sections, we will refer to  $Q = SE(3)$  as the configuration manifold for our system, and on this differentiable manifold we will formulate the equations of motion for a submerged rigid body, which will be presented as an affine connection control system.

In the body-fixed frame, we identify  $\boldsymbol{\nu} = (u, v, w)^t$  as the linear velocity and  $\boldsymbol{\Omega} = (p, q, r)^t$  as the angular velocity of the vehicle. We express these collectively as  $\mathbf{v} = (\boldsymbol{\nu}, \boldsymbol{\Omega})^t$ . If we define a rotation matrix  $R_2$  such that  $\boldsymbol{\eta}_2 = R_2 \boldsymbol{\Omega}$ , we can state the formulation of the kinematic equations of motion for a rigid body moving in six DOF as

$$\dot{\boldsymbol{\eta}} = \begin{bmatrix} R & 0_{3 \times 3} \\ 0_{3 \times 3} & R_2 \end{bmatrix} \begin{bmatrix} \boldsymbol{\nu} \\ \boldsymbol{\Omega} \end{bmatrix}. \quad (1)$$

Equivalently, formulating this system on the differentiable manifold  $Q$ , Eqs. (1) are written

as the *forward kinematic map*  $\Pi : Q \rightarrow \text{SE}(3)$ , with

$$\dot{\mathbf{b}} = R\boldsymbol{\nu}, \quad (2)$$

$$\dot{R} = R\hat{\Omega}. \quad (3)$$

In Eq. (3), the operator  $\hat{\cdot} : \mathbb{R}^3 \rightarrow \mathfrak{so}(3)$  is defined by  $\hat{\mathbf{y}}\mathbf{z} = \mathbf{y} \times \mathbf{z}$ . The space  $\mathfrak{so}(3)$  is the Lie algebra associated to the Lie group  $\text{SO}(3)$ , and is the space of skew-symmetric  $3 \times 3$  matrices (i.e.,  $\mathfrak{so}(3) = \{R \in \mathbb{R}^{3 \times 3} | R^t = -R\}$ ).

From standard references on rigid body dynamics (e.g., [14], [15], [16] and [17]), we have that the equations of motion for a submerged rigid body in an ideal fluid are given by

$$M_B \dot{\mathbf{v}} - \text{Cor}_B(\mathbf{v})\mathbf{v} = \boldsymbol{\sigma}(t), \quad (4)$$

where  $M_B$  and  $\text{Cor}_B$  respectively represent the rigid body inertia and the Coriolis and centripetal force matrices, and  $\boldsymbol{\sigma}(t)$  represents the external control forces. The external controls are the forces and moments applied by the actuators of the vehicle and can be written as  $\boldsymbol{\sigma} = (\boldsymbol{\varphi}_\nu, \boldsymbol{\tau}_\Omega)^t$ , where  $\boldsymbol{\varphi}_\nu = (X, Y, Z)^t$  and  $\boldsymbol{\tau}_\Omega = (K, M, N)^t$  and we adopt the standard SNAME notation for the forces  $(X, Y, Z)$  and moments  $(K, M, N)$ , [18].

To equivalently state Eqs. (4) using the geometric representation, we begin by expressing the translational ( $T_{\text{trans}}(t)$ ) and rotational ( $T_{\text{rot}}(t)$ ) portions of the body kinetic energy as

$$T_{\text{trans}}(t) = \frac{1}{2}m\|\dot{\mathbf{b}}(t)\|_{\mathbb{R}^3}^2, \quad T_{\text{rot}}(t) = \frac{1}{2}J_b\|\boldsymbol{\Omega}(t)\|_{\mathbb{R}^3}^2, \quad (5)$$

where  $m$  is the mass of the vehicle and  $J_b$  is its inertia. Now, let  $\gamma : \mathbb{R}^+ \rightarrow Q$  be a differentiable curve at  $q_0 \in Q$ . By use of the forward kinematic map  $\Pi : Q \rightarrow \text{SE}(3)$  we induce a differentiable curve  $\gamma_1 = \Pi \circ \gamma : \mathbb{R}^+ \rightarrow \text{SE}(3)$  at  $(\mathbf{b}_0, R_0) \triangleq \Pi(q_0)$ . If we assign a nonnegative number  $\text{KE}(\mathbf{v}_0)$  to the tangent vector  $\mathbf{v}_0 = \gamma'_{q_0} \in T_{q_0}Q$  ( $T_{q_0}Q$  is the tangent space to the manifold  $Q$  at  $q_0$ ), we define the kinetic energy of the rigid body at time zero along the curve  $\gamma_1$ . Repeating this process for every tangent vector  $\mathbf{v}$  and every point  $q$  of the manifold  $Q$ , we generate the function  $\text{KE} : TQ \rightarrow \mathbb{R}$ , which defines the kinetic energy. Here  $TQ$  is the union of all the tangent spaces, and is referred to as the *tangent bundle*. It is shown in [8] that there exists a  $C^\infty$ , positive-semidefinite tensor field  $\mathbb{G}$  such that  $\text{KE}(\mathbf{v}_q) = \frac{1}{2}\mathbb{G}(\mathbf{v}_q, \mathbf{v}_q)$ , which is analogous to the definition of the kinetic energy in  $Q = \text{SE}(3)$ . This  $\mathbb{G}$  is the inner product that we will

use in our equations.

Thus, the kinetic energy of a rigid body in an interconnected-mechanical system is represented by a tensor field on the configuration manifold  $Q$ . We refer to this object as the *kinetic energy metric* for the system. In a similar fashion, we can construct the kinetic energy for the fluid as another tensor field. The sum of the later and  $\mathbb{G}$  defines the total kinetic energy for the submerged rigid body.

To simplify both the standard and the geometric representations of the equations of motion, we make two non-limiting assumptions. First, we choose  $O_B$  to coincide with the center of mass of the AUV, and secondly, the axes of the body-fixed frame to correspond with the principle axes of inertia of the vehicle. These assumptions lead to  $M_B$  being a diagonal matrix.

Since the AUV is submerged in a viscous fluid we must introduce terms to account for the added mass, viscous damping and restoring forces. The added mass is a pressure-induced force due to the inertia of the surrounding fluid and is proportional to the acceleration of the rigid body. At low speed and assuming three planes of symmetry, as is common for most AUVs, the added mass matrix can be assumed to be diagonal,  $M_a = \text{diag}(M_f, J_f)$ .

Now, we have that the kinetic energy metric for the submerged rigid body is the unique Riemannian metric on  $Q = \text{SE}(3)$  given by:

$$\mathbb{G} = \begin{pmatrix} M & 0 \\ 0 & J \end{pmatrix}, \quad (6)$$

where  $M = mI_3 + M_f$  and  $J = J_b + J_f$ . In the sequel, we will use  $m_i = m + M_f^{\nu_i}$  and  $j_i = J_b^{\Omega_i} + J_f^{\Omega_i}$ , for  $i = 1, 2, 3$ . Thus,  $M = \text{diag}(m_1, m_2, m_3)$  and  $J = \text{diag}(j_1, j_2, j_3)$ .

As with any Riemannian metric, associated to  $\mathbb{G}$  is its *Levi-Civita affine connection*: the unique affine connection<sup>2</sup> that is both symmetric and metric compatible. The Levi-Civita connection (see e.g., [19]) provides the appropriate notion of acceleration for a curve in the configuration space by guaranteeing that the acceleration is in fact a tangent vector field along a curve  $\gamma$ . The connection also accounts for the Coriolis and centripetal forces acting on the system. Explicitly, if  $\gamma(t) = (\mathbf{b}(t), R(t))$  is a curve in  $\text{SE}(3)$ , and  $\gamma'(t) = (\boldsymbol{\nu}(t), \boldsymbol{\Omega}(t))$  is its pseudo-velocity as

<sup>2</sup>An affine connection transports tangent vectors to a manifold from one point to another along a curve.

given in Eqs. (2) and (3), the accelerations are given by

$$\nabla_{\gamma'}\gamma' = \begin{pmatrix} \dot{\boldsymbol{\nu}} + M^{-1}(\boldsymbol{\Omega} \times M\boldsymbol{\nu}) \\ \dot{\boldsymbol{\Omega}} + J^{-1}(\boldsymbol{\Omega} \times J\boldsymbol{\Omega} + \boldsymbol{\nu} \times M\boldsymbol{\nu}) \end{pmatrix}, \quad (7)$$

where  $\nabla$  denotes the Levi-Civita connection and  $\nabla_{\gamma'}\gamma'$  is the covariant derivative of  $\gamma'$  with respect to itself<sup>3</sup>. We refer to  $\nabla_{\gamma'}\gamma'$  as the *geometric acceleration* with respect to  $\nabla$  and note that Eq. (7) is Newton's Second Law expressed geometrically as  $a = \sum_i F_i/m$ .

To conclude this overview of the rigid body dynamics, note that Eq. (4) is equivalent to

$$\nabla_{\gamma'}\gamma' = \sum_{i=1}^6 \mathbb{I}_i^{-1}(\gamma(t))\sigma_i(t), \quad (8)$$

where the input control vector fields are the  $i$ -th column of the matrix

$$\mathbb{I}^{-1} = \begin{pmatrix} M^{-1} & 0 \\ 0 & J^{-1} \end{pmatrix}. \quad (9)$$

With no external forces  $\nabla_{\gamma'}\gamma' = 0$ , which represent the geodesics for the affine connection  $\nabla$ .

**Remark 1.** *It is important to note that the geometric acceleration is an effective way to consider acceleration in a general sense, as it is invariant under change of coordinates.*

Viscous damping and dissipation encountered by marine vehicles are caused by many factors, including radiation-induced potential damping from forced body oscillations in the presence of a free surface, linear and quadratic skin friction, wave drift damping, and vortex shedding. For a small, slow-moving, fully-submerged AUV which is far from the free surface, pressure drag (form drag) is dominant; this assumption is further validated based on the speed and shape of the test-bed vehicle considered here. Since we also assume that the AUV has three planes of symmetry, the hydrodynamic drag matrix is assumed diagonal and is given by  $D(\boldsymbol{v}) = \text{diag}(D_1\nu_1, D_2\nu_2, D_3\nu_3, D_4\Omega_1, D_5\Omega_2, D_6\Omega_3)$ . We assume that each of the viscous drag terms represented by  $D(\boldsymbol{v})\boldsymbol{v}$  to be quadratic with respect to the vehicle's velocity. Restoring forces and moments result from the effects of buoyancy and gravity upon the vehicle, and are represented by  $g(\boldsymbol{\eta})$ .

<sup>3</sup>Here we remind the reader that  $\nabla$  is not the submerged volume of fluid displaced by a rigid body, but denotes an affine connection on  $Q$ .

Incorporating the added mass terms and the viscous drag and restoring forces, we can extend Eq. (4) to

$$\begin{pmatrix} m\mathbb{I}_3 + M_f & 0_{3 \times 3} \\ 0_{3 \times 3} & J_b + J_f \end{pmatrix} \begin{pmatrix} \dot{\mathbf{v}} \\ \dot{\boldsymbol{\Omega}} \end{pmatrix} - D(\mathbf{v})\mathbf{v} - Cor_B(\mathbf{v})\mathbf{v} + g(\boldsymbol{\eta}) = \boldsymbol{\sigma}(t). \quad (10)$$

If we rewrite these equations in the standard Newton-Euler notation ( $F = ma$ ) and separate the translational and rotational motion components, we can express Eqs. (10) as

$$M\dot{\boldsymbol{\nu}} = -\boldsymbol{\Omega} \times M\boldsymbol{\nu} + D_{\boldsymbol{\nu}}(\boldsymbol{\nu})\boldsymbol{\nu} - g(\mathbf{b}) + \boldsymbol{\varphi}_{\boldsymbol{\nu}}, \quad (11)$$

$$J\dot{\boldsymbol{\Omega}} = -\boldsymbol{\Omega} \times J\boldsymbol{\Omega} - \boldsymbol{\nu} \times M\boldsymbol{\nu} + D_{\boldsymbol{\Omega}}(\boldsymbol{\Omega})\boldsymbol{\Omega} - g(\boldsymbol{\eta}_2) + \boldsymbol{\tau}_{\boldsymbol{\Omega}}, \quad (12)$$

where  $M\boldsymbol{\nu} \times \boldsymbol{\Omega}$  and  $J\boldsymbol{\Omega} \times \boldsymbol{\Omega}$  account for the Coriolis and centripetal forces.

Following this Newton-Euler formulation of the equations of motion, we can extend Eq. (8) and define the equations of motion for an underwater vehicle submerged in a viscous fluid in the framework of differential geometry using the Levi-Civita affine connection.

**Lemma 1.** *Let  $Q = \text{SE}(3)$ ,  $\nabla$  be the Levi-Civita connection on  $Q$  associated with the Riemannian metric  $\mathbb{G}$  and let the set of input control vector fields be given by  $\mathcal{I} = \{\mathbb{I}_1^{-1}, \dots, \mathbb{I}_6^{-1}\}$ . Let  $\mathbb{G}^\#(F_{drag}(\gamma'(t)))$  represent the dissipative forces resulting from hydrodynamic drag ( $\mathbb{G}^\#$  is the inverse of  $\mathbb{G}$ , and is a tangent bundle isomorphism physically meaning divide by mass). Let  $\mathbb{G}^\#(P(\gamma(t)))$  represent the restoring forces arising from gravity and buoyancy. Then the equations of motion of a rigid body submerged in a viscous fluid and subjected to dissipative and restoring forces are given by the forced affine connection control system:*

$$\nabla_{\gamma'}\gamma' = \mathbb{G}^\#(P(\gamma(t))) + \mathbb{G}^\#(F_{drag}(\gamma'(t))) + \sum_{i=1}^6 \mathbb{I}_i^{-1}(\gamma(t))\sigma_i(t), \quad (13)$$

where  $\sigma_i(t)$  represents the controls.

This concludes the general overview on the geometric control framework that will be used to generate the trajectories and control strategies for our test-bed vehicle. This overview, given with no intention of being comprehensive, has been presented to give the reader a notion regarding the concepts and tools that support the geometric control theory for AUVs. The focus of this paper remains upon the experimental results obtained through the practical implementation of

Mass	123.8 kg	$B = \rho g \mathcal{V}$	1215.8 N	$C_B$	(0, 0, -7) mm
Diameter	0.64 m	$W = mg$	1214.5 N	$C_G$	(0, 0, 0) mm
$M_f^u$	70 kg	$M_f^v$	70 kg	$M_f^w$	70 kg
$I_{xx}$	5.46 kg m <sup>2</sup>	$I_{yy}$	5.29 kg m <sup>2</sup>	$I_{zz}$	5.72 kg m <sup>2</sup>
$J_f^p$	0 kg m <sup>2</sup>	$J_f^q$	0 kg m <sup>2</sup>	$J_f^r$	0 kg m <sup>2</sup>

TABLE I  
MAIN DIMENSIONS AND HYDRODYNAMIC PARAMETERS FOR ODIN.

control strategies obtained by use of this geometric architecture. For a proof of Lemma 1 and an thorough analysis of geometric control theory applied to underwater vehicles, we refer the interested reader to [11].

#### A. Test-bed Platform: ODIN

To prove the effectiveness of our geometric path planning approach, we implemented the computed control strategies onto an agile and fully-actuated AUV; ODIN, see Fig. 3. Complete details and technical specifications for this vehicle can be found in [20] or [21], with specifics related to implementation of geometric control strategies contained in [11].

ODIN's main hull is a sphere constructed from anodized aluminum (AL 6061-T6). The numerical values of various parameters used for modeling ODIN are given in Table I. These values were derived from estimations and full-scale model tests performed on ODIN.

The added mass terms ( $M_f^u, M_f^v, M_f^w, J_f^p, J_f^q, J_f^r$ ) were estimated from formulas found in [22] and [23]. Moments of inertia ( $I_{xx}, I_{yy}, I_{zz}$ ) were calculated using experiments outlined in [24]. We used inclining experiments to locate  $C_G$ , which we take as the center of our body-fixed reference frame (i.e.,  $C_G = O_B$ ). Based on the symmetry of the vehicle, the center of buoyancy  $C_B$ , is assumed to be the center of the spherical body of ODIN. The location of  $C_B$  is measured from  $C_G = O_B$ , and is given in Table I.

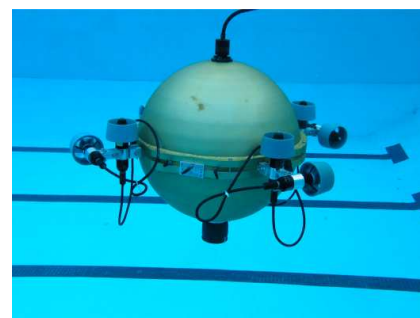


Fig. 3. ODIN operating in the pool.

Eight Tecnydyne brushless thrusters are attached to the sphere via four fabricated mounts, each holding two thrusters. These thrusters are evenly distributed around the sphere with four

oriented vertically and four oriented horizontally. This design provides instantaneous and unbiased motion in all six DOF, contrary to the more common torpedo-shaped vehicles. Unique to ODIN's construction is the control from an eight-dimensional thrust to move in six DOF. Hence, ODIN operates in an over-actuated condition; redundancy was incorporated in the design to account for thruster failure or other operational errors. To calculate the six-dimensional thrust  $\sigma$  resulting from the eight-dimensional thrust  $\zeta$  (from the thrusters), or vice-versa, we apply a linear transformation to  $\zeta$ . We omit the details of this transformation here, but refer the interested reader to [20]. Along with the tests to determine the values in Table I, we also tested the thrusters. Each thruster has a unique voltage input to power output relationship. This relationship is highly nonlinear and is approximated using a piecewise linear function which we refer to as our thruster model. More information regarding the thruster modeling can be found in [11].

Major internal components include a pressure sensor, inertial measurement unit, leakage sensor, heat sensor and 24 batteries (20 for the thrusters and four for the CPU). ODIN is able to compute and communicate real-time, yaw, pitch, roll, and depth, and can operate for up to five hours from either a tethered or fully-autonomous mode.

ODIN does not have real time sensors to detect horizontal ( $x-y$ ) position. Instead, experiments are videotaped from a platform 10 m above the water's surface, giving us a near nadir view of ODIN's movements. Videos are saved and horizontal position data are post-processed for later analysis. A real-time system utilizing sonar was available on ODIN, but it has not been used in these experiments mainly for two reasons. First, the sonar created too much noise in the diving well and led to inaccuracies. More significantly, in the implementation of our control strategies, ODIN is often required to achieve large ( $> 15^\circ$ ) list angles which render the sonars useless for horizontal positioning. Many alternative solutions were attempted and video provided a cost-effective solution which produced accurate results. We are able to determine ODIN's relative position in the testing pool to  $\pm 10$  cm.

For the applications motivated in the following sections, we additionally assume that ODIN has a forward facing camera (or other data collecting sensor) mounted at the equator of the spherical hull. This is the sensor that will be used to examine the ship's hull.

### III. CONTROL STRATEGY DESIGN

As previously mentioned, the aim of this paper is to present a path planning approach with experimental trials to provide solutions to the problem of surveying a complicated section of a ship's hull, i.e., the bulbous bow. To this end, we are interested in calculating paths that the AUV can execute given its controllability, and subsequently computing the controls to be applied by the actuators to realize the chosen path. Hence, the path planning problem is solved based on the actuation constraints of the vehicle, and the controls are computed by solving the kinematic motion planning problem for the prescribed path. This control strategy design process was developed by following a differential geometric procedure outlined in [8] in a very general manner and in [10] for application to AUVs. The detailed process of adapting the computed controls for implementation onto the considered test-bed vehicle is described in [11]. To summarize this procedure, we begin by first applying a geometric reduction procedure to the dynamic system (acceleration control inputs) described by Eqns. (13) to produce a kinematic (velocity control inputs) control system. We then calculate the decoupling vector fields for this kinematic system. A decoupling vector field is a vector field whose integral curves (under any reparameterization) are solutions to the kinematic system as well as the dynamic system. In particular, the integral curves of the decoupling vector fields define trajectories for the kinematic system that can be extended to realizable trajectories of the dynamic system. Thus, by use of decoupling vector fields, we are able to solve the motion planning problem for the kinematic system. By Theorem 13.2 in [8], it is guaranteed that this solution can be extended to a solution for the dynamic system. The decoupling vector fields for a given system are based on the actuation and controllability of the system. For a fully-actuated vehicle, as presented here, every vector field is decoupling. However, for an under-actuated vehicle (e.g., torpedo-shaped vehicle) the decoupling vector fields have to be calculated, and there may exist configurations that are unreachable by kinematic motions due to a vehicle's controllability constraints.

Heuristically, this geometric reduction technique is similar to solving a second-order differential equation by substitution of variables. Although this method may not find *all* solutions to the motion planning problem for the dynamic system, we are able to calculate some solutions without explicitly solving the complete dynamic system. Once we have chosen the integral curves of the decoupling vector fields that connect the initial and final configurations, we reparameterize and

concatenate them to define the trajectory for the vehicle to follow. The corresponding control strategy to realize this trajectory is calculated via inverse kinematics by applying Theorem 13.5 in [8] and the extension of this result presented in [11].

We continue by briefly outlining the procedure of motion planning via decoupled kinematic motions. First, we define the initial ( $\eta_{init}$ ) and final ( $\eta_{final}$ ) configurations of the system. We make the assumption that either the initial configuration is the current one or is realizable by the vehicle, otherwise the problem is not well stated.

This trajectory design process is based on what is commonly known in control literature as *motion planning by use of primitives*. This involves the concatenation of several calculated primitives to create a realizable path connecting  $\eta_{init}$  and  $\eta_{final}$ . The time-parameterized, concatenated path then defines the trajectory from  $\eta_{init}$  to  $\eta_{final}$ . Determining whether or not the final configuration is reachable by use of only the kinematic motions defined by the decoupling vector fields for the given system is non-trivial. We refer the reader to [10] for a complete characterization of decoupled vector fields, and the corresponding controllability of the system.

After solving the motion planning problem by determining the sequence of integral curves, or primitives, to follow to get from  $\eta_{init}$  to  $\eta_{final}$ , we parameterize each segment to start and end at zero velocity. This parameterization ensures that each concatenated segment begins with the same initial conditions, and thus guarantees that the entire motion is executable by the vehicle. From this reparameterized, concatenated, kinematic motion trajectory, we calculate the dynamic controls that steer the vehicle from  $\eta_{init}$  to  $\eta_{final}$ . With this heuristic blueprint in mind, we now present the details of the construction.

Suppose that we have a  $C^\infty$  affine connection control system  $\Sigma_{dyn} = (Q, \nabla, \mathcal{I}^{-1}, \mathbb{R}^m)$ , where  $m$  is defined by the number of available DOF. Let the system  $\Sigma_{dyn}$  be kinematically controllable, in other words, the system can reach any arbitrary final configuration (with zero velocity) from any initial configuration (with zero velocity) by use of kinematic motions. First, calculate the decoupling vector fields for the drift-less kinematic system  $\Sigma_{kin} = (Q, \mathcal{V} = \{V_1, \dots, V_m\}, \mathbb{R}^m)$ . This is a straightforward calculation for a given system by following the general outline in [8]. Based on various actuation scenarios for ODIN, a complete characterization of its decoupling vector fields is presented in [10].

Let  $\mathcal{F}_t^{V_i}$  represent the flow along the integral curve of the vector field  $V_i$  for a duration  $[0, t]$ . Set the initial configuration as  $\eta_{init}$  and the final configuration as  $\eta_{final}$ . Next, solve the kinematic

motion planning problem by concatenating the flows of the decoupling vector fields from  $\eta_{init}$  to  $\eta_{final}$  by finding  $k \in \mathbb{N}$ ,  $a_1, \dots, a_k \in \{1, \dots, m\}$ ,  $t_1, \dots, t_k \in \mathbb{R}^+$  and  $\epsilon_1, \dots, \epsilon_k \in \{1, -1\}$  such that

$$\mathcal{F}_{t_k}^{\epsilon_k V_{a_k}} \circ \dots \circ \mathcal{F}_{t_1}^{\epsilon_1 V_{a_1}}(\eta_{init}) = \eta_{final}. \quad (14)$$

For each  $j \in \{1, \dots, k\}$ , choose a  $C^2$ -reparameterization  $\tau : [0, \bar{t}_j] \rightarrow [0, t_j]$  such that  $\tau'(0) = \tau'(\bar{t}_j) = 0$  so that the kinematic motion begins and ends at rest (zero velocity). Define  $\gamma : [0, t_j] \rightarrow Q$  as the integral curve  $t \mapsto \mathcal{F}_t^{\epsilon_j V_{a_j}}$ . Then the dynamic control  $\sigma : [0, \bar{t}_j] \rightarrow \mathbb{R}^m$  is defined by

$$\sum_{\alpha=1}^m \sigma_\alpha(t) \mathbb{I}_\alpha^{-1}(\gamma \circ \tau(t)) = (\tau'(t))^2 \nabla_{V_{a_j}} V_{a_j}(\gamma \circ \tau(t)) + \tau''(t) V_{a_j}(\gamma \circ \tau(t)). \quad (15)$$

If we let  $u : [0, T] \rightarrow \mathbb{R}^m$  be the control formed by the concatenation of  $\sigma_1, \dots, \sigma_k$ , then  $(\gamma, u)$  is a controlled trajectory for  $\Sigma_{dyn}$ . This general method of calculating the controls for a dynamic system following decoupling vector fields was adapted from [8] for our specific application.

Note that for the experiments presented in Section IV, we considered ODIN to be fully-actuated. Therefore every kinematic motion can be generated as dynamic motion using Eq. (15).

**Remark 2.** *Inherent to this trajectory design technique, the speed along each concatenated integral curve can arbitrarily be chosen, thus the parameterization depends upon the physical limits of the thrusters or actuators of the given vehicle. Additionally, with different choices of  $\tau(t)$ , to some extent, we can control the time and energy efficiency of the vehicle over the duration of a given path. However, if the calculated trajectory requires the concatenation of two or more integral curves, we can never achieve time optimality between the initial and final configurations. This is a direct result of the trajectory segments being concatenated through states of zero velocity; obviously such a strategy can never be time optimal.*

Unfortunately, in their current form, the calculated controls cannot be directly implemented onto ODIN. This however, does not imply that these strategies cannot be implemented directly onto an alternative test-bed vehicle. The geometric control theory technique generates continuous controls as a function of time, whereas ODIN's input requires a piece-wise constant control structure over discretized time intervals. The reason for this type of input is based on the combination of the refresh rate of the controller and the voltage to thrust relation used for

ODIN's thrusters. Also, it is important to keep the thrusters operating in a steady state to reduce their transient output response from constant changes in input voltage. In addition to this unique control structure, we must also link the piece-wise constant thrusts via a linear function, since it is impossible for a physical actuator to change outputs instantaneously.

Hence, to test our designed control strategies on ODIN, we must adapt the continuous control strategies into piece-wise constant (PWC) control strategies. To do this, we consider the work that is required to perform a desired motion, and ensure that equivalent work is being done by both the continuous and PWC controls. The work done on the system over a given time interval is calculated by integrating the control with respect to time. Thus, by appropriately choosing the times when the actuator switches from one PWC to another, we can design a PWC control from a given continuous control where the work done on the system is equivalent. This process is best explained via the following example.

**Example 1.** *Consider the simple motion of a five meter pure surge relative to the body-fixed reference frame. If we assume that  $\eta_{init} = (0, 0, 0, 0, 0, 0)$ , then  $\eta_{final} = (5, 0, 0, 0, 0, 0)$ . Since ODIN is assumed to be fully-actuated, we have control over all six DOF. This implies that we have six input control vector fields  $\mathcal{I}_6^{-1} = \{\mathbb{I}_1^{-1}, \mathbb{I}_2^{-1}, \mathbb{I}_3^{-1}, \mathbb{I}_4^{-1}, \mathbb{I}_5^{-1}, \mathbb{I}_6^{-1}\}$ , and every vector field is a decoupling vector field. Hence, the decoupling vector fields for this system are the constant multiples and linear combinations of the set  $\mathcal{D} = \{X_1 = (1, 0, 0, 0, 0, 0), X_2 = (0, 1, 0, 0, 0, 0), X_3 = (0, 0, 1, 0, 0, 0), X_4 = (0, 0, 0, 1, 0, 0), X_5 = (0, 0, 0, 0, 1, 0), X_6 = (0, 0, 0, 0, 0, 1)\}$ .*

*To achieve the desired motion, we need only consider integral curves of the decoupling vector field  $X_1$ . Here, there is only one integral curve to follow, and  $\mathcal{F}_5^{X_1}(\eta_{init}) = \eta_{final}$ . Thus, the trajectory  $\gamma(t) : [0, 5] \rightarrow Q$  is simply the straight line from  $(0, 0, 0, 0, 0, 0)$  to  $(5, 0, 0, 0, 0, 0)$ . For this example, we choose to reparameterize  $\gamma(t)$  using  $\tau(t) : [0, 30] \rightarrow [0, 5]$  so that the motion lasts for 30 seconds. This reparameterization gives an average velocity for the trajectory of 0.167 m/s. From the data and analysis presented in [11], the drag coefficient applicable for this motion is  $D_1 = 231$  kg/m. Hence, we can calculate the dynamic control structure by use of Eq. (15) as*

$$\sigma^1(t)\mathbb{I}_1^{-1}(\gamma \circ \tau(t)) = (\tau'(t))^2 \widetilde{\nabla}_{X_1} X_1(\gamma \circ \tau(t)) + \tau''(t)X_1(\gamma \circ \tau(t)), \quad (16)$$

where  $\tau(t) = \frac{t^2(45-t)}{2700}$ , which ensures that the vehicle will begin and end the motion with zero

velocity. Computing the covariant derivative, Eq. (16) becomes

$$\begin{aligned}\sigma^1(t) &= D_1(\tau'(t))^2 + m_1\tau''(t) \\ &= 231 \left( \frac{t(30-t)}{900} \right)^2 + 196 \left( \frac{15-t}{450} \right) \\ &= \frac{7(11t^4 - 660t^3 + 9900t^2 - 16800t + 252000)}{270000}.\end{aligned}\tag{17}$$

Thus, the control strategy calculated by use of our geometric methods for realizing a pure surge displacement of five meters for ODIN is given by  $\sigma^1(t) = \frac{7(11t^4 - 660t^3 + 9900t^2 - 16800t + 252000)}{270000}$ . This control has a positive portion to accelerate the vehicle from rest and realize the motion and a negative section to slow the vehicle to a complete stop in the prescribed location. The value of  $\sigma^1(t)$  is zero at  $t = 0, 25.05$  and  $30$  seconds. For implementation onto ODIN, we need to convert  $\sigma^1(t)$  into a PWC control. Consider,

$$s_1 = \frac{1}{25.05} \int_0^{25.05} \sigma^1(t) dt, \quad s_2 = \frac{1}{4.95} \int_{25.05}^{30} \sigma^1(t) dt.\tag{18}$$

Calculating, we get  $s_1 = 9.98 \text{ N}$  and  $s_2 = -3.84 \text{ N}$ . Thus, we can write the PWC control as

$$s^1(t) = \begin{cases} 9.98 \text{ N} & t \in [0, 25.05] \\ -3.84 \text{ N} & t \in [25.05, 30] \end{cases}.\tag{19}$$

The final step to implement this onto ODIN is to simply connect these two constant controls via a linear junction lasting 0.9 seconds to avoid instantaneous switching of the thrust command sent to the thrusters. The duration of this junction is based upon the refresh rate of ODIN's CPU and the avoidance of large voltage changes which may damage ODIN's thrusters (see [20] for detailed information).

The resulting discretized control structure which is implemented onto ODIN is listed in Table II, where the six-dimensional control structure is given by  $\sigma = (\sigma^1, \sigma^2, \dots, \sigma^6)$ .

At this point, we merge theory and application together through the implementation of the computed control strategies onto ODIN. Algorithm 1 presents the overall method for designing and implementing our control strategies.

Time (s)	Applied Thrust (6-dim.) (N)
0	(0,0,0,0,0,0)
0.9	(9.98,0,0,0,0,0)
25.95	(9.98,0,0,0,0,0)
26.85	(-3.84,0,0,0,0,0)
31.8	(-3.84,0,0,0,0,0)
32.7	(0,0,0,0,0,0)

TABLE II  
DISCRETIZED CONTROL STRUCTURE FOR 5M PURE SURGE.

---

**Algorithm 1** Implementation of Control Strategies Designed using Differential Geometry

---

- 1: Apply a kinematic reduction to Eqs. (13).
  - 2: Solve the motion planning problem from  $\eta_{init}$  to  $\eta_{final}$  via inverse kinematics.
  - 3: Calculate the continuous control strategy  $\sigma(t)$  for the dynamic system by use of the geometric theory, i.e., Eq. (15).
  - 4: Discretize  $\sigma(t)$  to obtain an implementable piece-wise constant control structure  $\sigma_0(t)$ .
  - 5: Upload  $\sigma_0(t)$  to ODIN's CPU.
  - 6: **while** ODIN autonomously implements  $\sigma_0(t)$  in full open-loop. **do**
  - 7:   On-board, ODIN converts  $\sigma_0(t)$  from a 6-dimensional control to an 8-dimensional control.
  - 8:   The 8-dimensional control is converted from force (N) to voltage (V).
  - 9:   The voltage controls are send to the eight independent thrusters.
  - 10:   Position and orientation data are collected.
  - 11: **end while**
  - 12: Collected data are post-processed and analyzed
- 

#### IV. EXPERIMENTS

In the sections to follow, we present experimental results for three geometrically designed control strategies to survey portions of a ship's bulbous bow. Since the shape of the bulb affects the performance of the vessel at sea, each bulb is uniquely constructed for an individual ship and many different shapes and sizes are seen in use today. However, a general bulb can be approximated by a cylindrical solid capped by a hemisphere. We will assume this simplified scenario for our experiments. Note that small perturbations in the shape of the bulb will not greatly affect the design of our paths or the associated controls. Additionally, for very unique bulb shapes, and to implement these techniques at full-scale, similar methods to those described here can be employed to design specific trajectories and control strategies. Figure 4 displays a

typical bulbous bow, along with relative dimensions.

To reiterate, during the experiments, the computed control strategies were implemented in full open-loop fashion, thus there are no feedback controllers in operation. Due to this mode of operation, we expect and notice deviations between the prescribed path and the actual implemented trajectory. There are multiple reasons for such deviations, and we explicit them when discussing each implementation result. Open-loop control implementation is not our intention for a vehicle performing a real-world mission, but it has been chosen to demonstrate the effectiveness of the technique used to design the control strategies. Implementing the computed control in conjunction with a standard adaptive or feedback controller will result in an effective control system for AUVs to survey ship hulls.

To survey the uniquely-shaped bulbous bow, we propose two separate missions. The first is a semi-circular trajectory as depicted in Fig. 5. Here, the vehicle performs a pure heave while simultaneously applying a pure surge. This trajectory can be used to survey the front of the bulb, as seen in Fig. 8, or to perform repeated transects up and down the longitudinal axis of the bulb, as shown in Fig. 6. The second trajectory considered to survey a bulbous bow is a motion parallel to the free surface while maintaining a desired pitch angle to point the front-mounted camera, or sensor, at the surface of the bulb. This trajectory is depicted by the line parallel to the load water line (LWL) in Fig. 7. The third proposed strategy is the concatenation of the previous two, as seen Fig. 8. We now continue by presenting the computed controls and the implementation results for these missions.

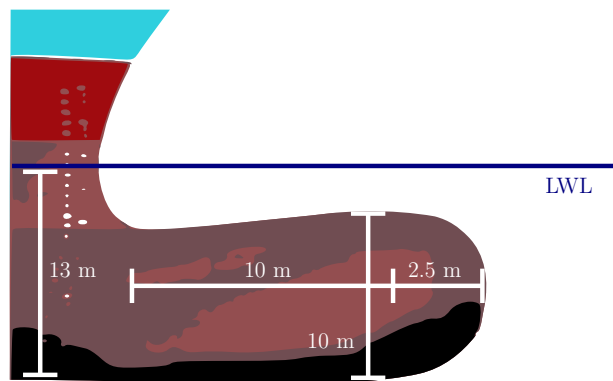


Fig. 4. Side view of a bulbous bow on a ship and its dimension.

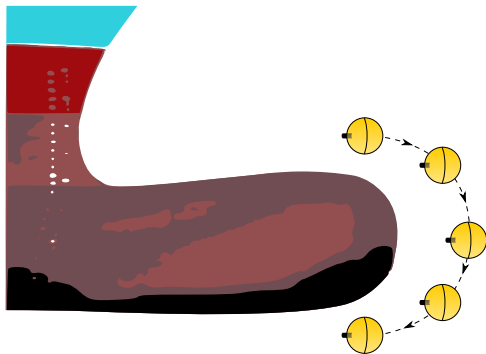


Fig. 5. Side view of a bulbous bow on a ship. Also depicted is the semi-circle trajectory for the inspection of the front of a bulbous bow.

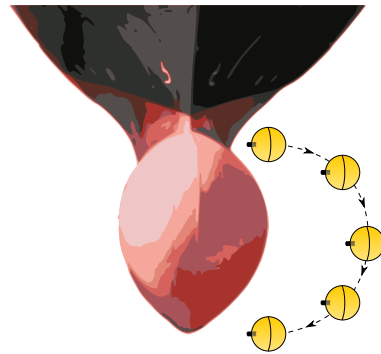


Fig. 6. Front view of a bulbous bow. Also depicted is the trajectory to survey the sides of the bulb.

For all of the experiments, the initial configuration is taken to be  $\eta_{init} = (0, 0, 1.5, 0, 0, 0)$ , with the origin of the earth-fixed frame positioned on the free surface. In particular,  $\eta_{init}$  is located at the origin of the earth-fixed frame, 1.5 m below the water's surface. All control strategies presented here are designed such that the vehicle begins at  $\eta_{init}$  with zero velocity, and ends at  $\eta_{final}$  with zero velocity. The presented experiments were performed in the diving well at the Duke Kahanamoku Aquatic Complex at the University of Hawai'i. As such, we are unable to perform strategies that are full-scale with respect to the dimensions shown in Fig. 4. We scale the height of the bulb from 10 m to 2.5 m, which implies that the 2.5 m radius of the hemisphere scales to approximately 0.5 m. For the motion parallel to the free surface, we scale the 10 m length of the bulb to 5 m. As the aim of this paper is to present the implementation results of control strategies computed via differential geometric techniques, we omit the details of the calculation of each control strategy, and simply present the PWC controls that were executed by ODIN. The calculations are similar to those carried out in Example 1, and the interested reader is directed to [11] for detailed calculations of multiple control strategies.

#### A. Strategy One: Semi-circle

The first strategy we wish to construct is the semi-circle trajectory shown in Fig. 5, to inspect the front and the sides of the bulbous bow. This motion is constructed by simultaneously applying

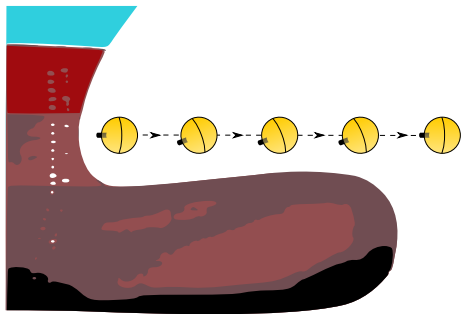


Fig. 7. Side view of a bulbous bow on a ship. Also depicted is the linear trajectory for the inspection of the top of a bulbous bow.

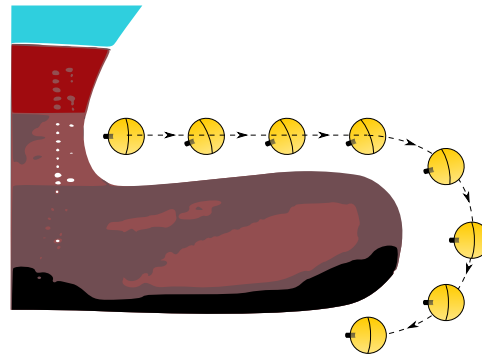


Fig. 8. Overall path for complete inspection of a bulbous bow.

controls in both pure heave and pure surge. The pure heave control is designed so that the vehicle realizes a net 2.5 m pure heave. The surge control is designed such that the vehicle begins at rest, realizes a negative pure surge of 0.5 m, then moves 0.5 m in the positive surge direction to culminate with zero net displacement in pure surge. The final configuration for the vehicle is  $\eta_f = (0, 0, 4, 0, 0, 0)$  meters. We parameterize this motion to begin and end at rest, and based on the operational velocity of ODIN, the duration of the motion is 10.7 seconds. We present the computed PWC control strategy in Table III as a six-dimensional control, corresponding to the six DOF in the body-fixed reference frame.

Time (s)	Applied Thrust (6-dim.) (N)	Time (s)	Applied Thrust (6-dim.) (N)
0	(0,0,0,0,0,0)	6.5	(32.7, 0, 30.04, 0, 0, 0)
0.9	(-32.7, 0, 30.04, 0, 0, 0)	7.7	(32.7, 0, -24.56, 0, 0, 0)
2.8	(-32.7, 0, 30.04, 0, 0, 0)	8.6	(-30.99, 0, -24.56, 0, 0, 0)
3.7	(30.99, 0, 30.04, 0, 0, 0)	9.8	(-30.99, 0, -24.56, 0, 0, 0)
4.9	(30.99, 0, 30.04, 0, 0, 0)	10.7	(0,0,0,0,0,0)
5.8	(32.7, 0, 30.04, 0, 0, 0)		

TABLE III  
PIECE-WISE CONSTANT CONTROL STRATEGY TO PERFORM A SEMI-CIRCLE TRAJECTORY.

Figure 9 displays the implementation results of the control strategy given in Table III. The

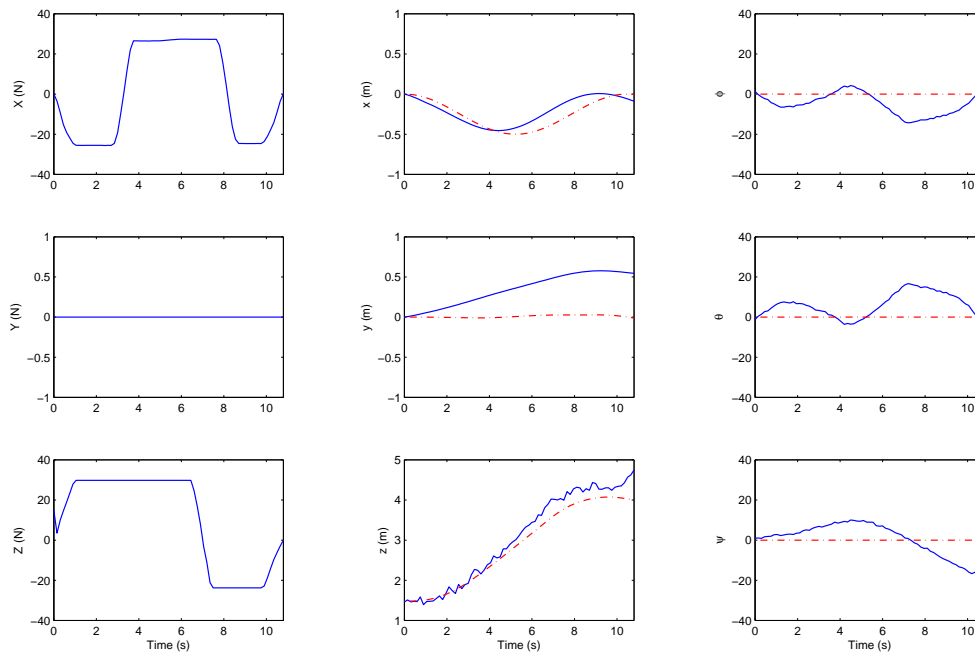


Fig. 9. Strategy One: Semi-circle trajectory. Solid (blue) line represents actual evolution, dash-dot (red) line represents the theoretical evolution.

first column of plots in Fig. 9 give the control forces (in Newtons) that were applied by ODIN during the implementation. In the second and third columns, we display the evolution of all six DOF of the vehicle during the test. The solid (blue) line denotes the actual evolution of ODIN. The dash-dot (red) line represents the theoretical evolution of ODIN. The theoretical evolution represents the trajectory that ODIN was prescribed to follow based on the concatenated integral curves that were chosen to solve the motion planning problem.

First, we examine the controls applied during the experiment. Note that for the surge control  $X$ , the magnitude of the control does not quite match the values given in Table III. This is a result of implementing a six-dimensional control strategy onto a vehicle that is driven by eight thrusters. The linear transformation applied to convert from six dimensions to eight dimensions, and vice-versa, has a nonzero null space. This means that there are infinitely many transformations which convert the controls. ODIN's on-board computer chooses one of these transformations for its computations. More information regarding this transformation can be found in [11], with specific

details related to ODIN found in [25]. We remark that ODIN performs this transformation twice during the implementation. First, ODIN computes the 8-dimensional thrust from the prescribed six-dimensional controls. After implementation, ODIN transforms the actual applied controls from the eight thrusters into a six-dimensional output control for post-processing.

Next, consider the evolution of ODIN during the experiment. The main intent of this strategy was to realize both heave and surge motions. For the surge motion, the experimental results match well with the theoretical trajectory. We see deviation between the actual and theoretical evolutions begin around  $t = 4$  seconds. This occurs because ODIN did not reach the full 0.5 m displacement. The actual evolution is seen to be just out of phase of the theoretical prediction. This is probably a result of a small error in the drag coefficient calculated for ODIN. Overall, the surge motion was executed very well. Similarly for the heave motion, we see an excellent correspondence between theoretical predictions and experimental results. The sway motion displays a slight deviation, which is a result of an initial yaw angle offset at the beginning of the experiment. Such an offset cannot be corrected since we are operating in open-loop. This type of implementation coupled with potential transient thruster response results in the discrepancies seen in the plots for the Euler angles. Such discrepancies are minimal and expected. Research is active in the design of a robust feedback controller for AUVs to track a given trajectory in the presence of initial disturbances such as yaw offsets and disturbance inputs. Initial results in this area can be found in [12] and [13]. It is an area of future work to implement such a controller onto ODIN for trajectory tracking experiments.

### *B. Strategy Two: Horizontal Survey*

The second strategy we implemented is a common control strategy for a seabed survey for applications such as coral reef monitoring. It is simply composed of a pitch angle of  $\theta = -20^\circ$  and a five meter surge while maintaining this pitch angle and constant depth.<sup>4</sup>

This control strategy provides the ability to survey the top of the bulb, while choosing  $\theta = 20^\circ$  and moving in the positive surge direction will allow for survey of the bottom of the bulb. The basic idea for this control strategy is to pitch the vehicle so that the forward-looking camera (or sensor) points downward, then apply a pure surge control (relative to the earth-fixed reference

<sup>4</sup>The pitch angle of  $-20^\circ$  is chosen based on the physical limitations of the test-bed vehicle ODIN.

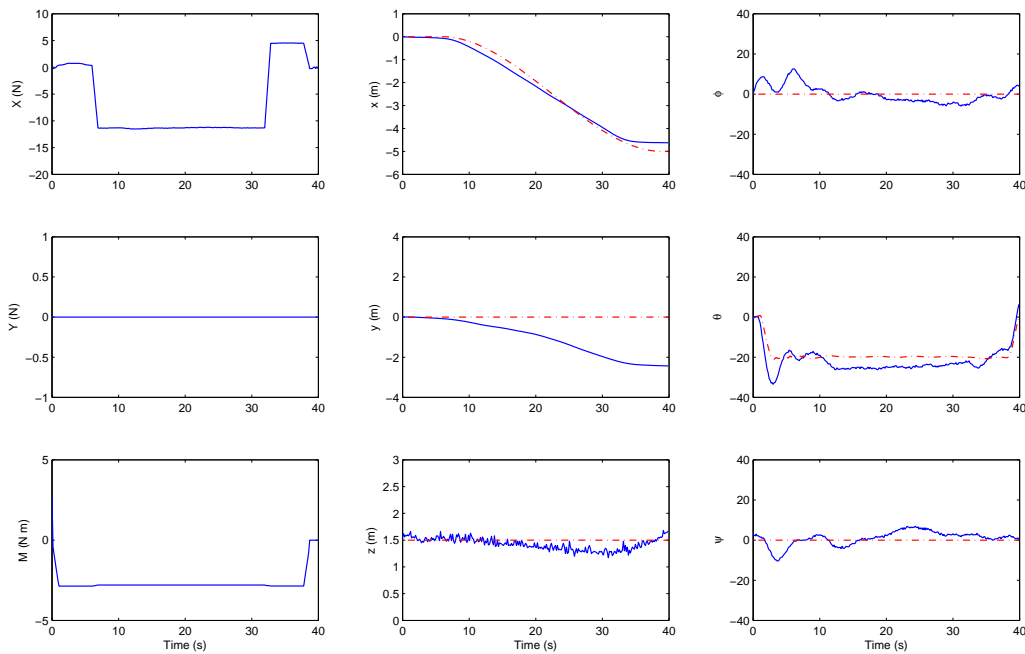


Fig. 10. Strategy Two: Horizontal survey. Solid (blue) line represents actual evolution, dash-dot (red) line represents the theoretical evolution.

frame) while maintaining the desired pitch angle to survey along top or bottom of the bulb. In this case, we prescribe a  $-5$  m pure surge and a final configuration for the vehicle of  $\eta_f = (-5, 0, 1.5, 0, -20^\circ, 0)$ . The duration of this motion is 38.6 seconds. The six-dimensional PWC control strategy is given in Table IV.

Time (s)	Applied Thrust (6-dim.) (N)	Time (s)	Applied Thrust (6-dim.) (N)
0	(0,0,0,0,0,0)	31.9	(-10.7, 0, 7.6, 0, -2.91, 0)
0.9	(0.45, 0, 1.2, 0, -2.91, 0)	32.8	(4.6, 0, 2.02, 0, -2.91, 0)
5.9	(0.45, 0, 1.2, 0, -2.91, 0)	37.7	(4.6, 0, 2.02, 0, -2.91, 0)
6.8	(-10.7, 0, 7.6, 0, -2.91, 0)	38.6	(0,0,0,0,0,0)

TABLE IV  
PIECE-WISE CONSTANT CONTROL STRATEGY TO SURVEY THE TOP PORTION OF THE BULBOUS BOW.

For this implementation, we had issues with yaw stabilization throughout implementation of

the control strategies and frequently had large deviations at the culmination of the mission. To compensate for this, we employed a feedback controller for only the yaw control. ODIN has a Proportional-Derivative (PD) controller on-board, which can be activated to provide feedback in depth, roll, pitch and/or yaw. ODIN does not have an on-board compass, so yaw angles, and associated errors, are measured relative to the yaw angle at the initialization of the motion, which is assumed to be zero. This initial angle is what the feedback controller is working to maintain. In Fig. 10, we see a large deviation in sway ( $y$ ) due to the feedback controller maintaining a non-zero yaw angle throughout implementation the experiment. Note that during the first  $\sim 8$  seconds, the vehicle should be performing a pure pitch, however we notice artifacts in the roll evolution, also caused by this initial yaw angle offset. The deviation in sway begins to appear when the vehicle executes the translational portion of the implementation. Since we supply the controls to realize a given motion in open-loop, and ODIN has no on-board sensors for horizontal positioning, running a feedback control loop on yaw alone will not eliminate deviation in sway caused from such an initialization error. Additionally, since the horizontal positioning is decoupled from the actual vehicle, they may have slightly different frames of reference based on the assumed initial yaw angle. In particular, a translational motion relative to the vehicle may differ from a translational motion relative to the camera atop the diving platform. Additional results for this implementation are presented in Fig. 10, and our discussion continues with considering the evolution of other parameters.

The initial seven seconds of this strategy is devoted to stabilize the pitch angle to the prescribed  $-20^\circ$ . During this time we see that the  $x$ ,  $y$  and  $z$  evolutions remain stable with some disturbance seen in  $\phi$ . The pitch angle did not quite stabilize during the initial seven seconds, but it quickly levels out from about  $t = 12$  seconds onward. Note that this pitch angle is slightly more than the  $-20^\circ$  prescribed. This excess pitch attributes to the slight rise to the surface seen in the depth evolution. Regardless, the actual depth evolution remains around the prescribed 1.5 m for the duration of the trajectory. For the surge evolution, we see that ODIN approximately realized the predicted 5 m displacement. Error here is again due to an error in the estimation of the drag coefficients for the vehicle. Overall, the implementation of this control strategy matched well with the desired trajectory to be performed.

### C. Strategy Three: Concatenated Motion

Here, we combine the control strategies presented in Sections IV-A and IV-B into a single implementable trajectory. Since both of the previous strategies were designed to begin and end at rest, we can simply concatenate them together. The final configuration for this motion is  $\eta_f = (-5, 0, 4, 0, 0, 0)$ , which is realized over a duration of 49.3 seconds. The six-dimensional PWC control strategy is given in Table V.

Time (s)	Applied Thrust (6-dim.) (N)	Time (s)	Applied Thrust (6-dim.) (N)
0	(0,0,0,0,0,0)	42.3	(30.99, 0, 30.04, 0, 0, 0)
0.9	(0.45, 0, 1.2, 0, -2.91, 0)	43.5	(30.99, 0, 30.04, 0, 0, 0)
5.9	(0.45, 0, 1.2, 0, -2.91, 0)	44.4	(32.7, 0, 30.04, 0, 0, 0)
6.8	(-10.7, 0, 7.6, 0, -2.91, 0)	45.1	(32.7, 0, 30.04, 0, 0, 0)
31.9	(-10.7, 0, 7.6, 0, -2.91, 0)	46	(32.7, 0, -24.56, 0, 0, 0)
32.8	(4.56, 0, 5.02, 0, -2.91, 0)	46.3	(32.7, 0, -24.56, 0, 0, 0)
37.7	(4.56, 0, 5.02, 0, -2.91, 0)	47.2	(-30.99, 0, -24.56, 0, 0, 0)
38.6	(-32.7, 0, 30.04, 0, 0, 0)	48.4	(-30.99, 0, -24.56, 0, 0, 0)
41.4	(-32.7, 0, 30.04, 0, 0, 0)	49.3	(0,0,0,0,0,0)

TABLE V  
PIECE-WISE CONSTANT CONTROL STRATEGY FOR THE CONCATENATION OF THE TWO STRATEGIES PRESENTED IN SECTIONS IV-A AND IV-B.

The general idea for this strategy is that the vehicle begins above the bulb and close to the bow of the ship, it pitches to point the camera downward, then traverses the length of the bulb parallel to the free surface. Upon reaching the end of the bulb, the AUV performs the semi-circle motion to examine the front portion of the bulb. For this concatenated strategy, we choose not to apply controls at the end of the initial segment to undo the prescribed pitch angle. This is done in an attempt to create the effect seen in Fig. 8, where the camera points nearly normal to the surface of the bulb for the first half of the semi-circle trajectory.

Note that the concatenation of two control strategies can give different results from those obtained by implementing each individually. This is directly related to the ability to stabilize the vehicle at the junction connecting the two strategies. Based upon the design of the control strategies, each segment of the concatenation should begin and end with zero velocity, thus making the concatenation feasible. However, this does not always occur in practice. Additionally, any errors present in the implementation of the initial leg of the concatenated motion are

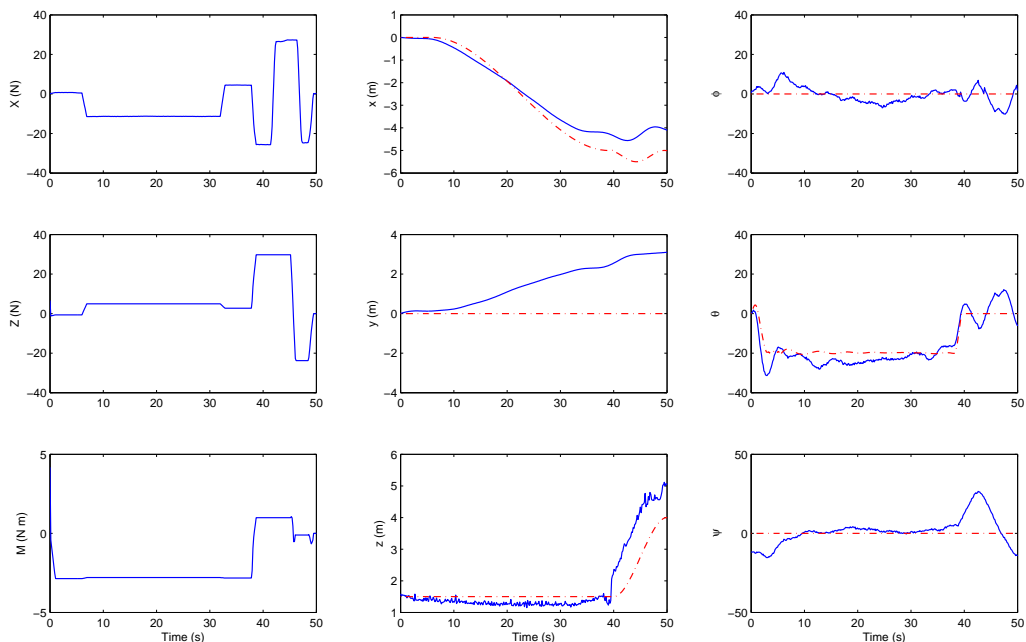


Fig. 11. Strategy Three: Concatenation of the semi-circle trajectory and the horizontal survey. Solid (blue) line represents actual evolution, dash-dot (red) line represents the theoretical evolution.

exaggerated through execution of subsequent portions since the initialization point of the later motions is not in the prescribed location. In an effort to perform concatenated strategies well, we again activated a feedback controller for the yaw control for this experiment.

The initial 40 seconds of the implementation displayed in Fig. 11 is the strategy presented in Section IV-B, while the remainder of the experiment is the semi-circle strategy presented in Section IV-A. During the initial segment of the trajectory, we see similar results to those described in Section IV-B. The depth remains fairly constant at 1.5 m, the AUV realizes approximately 5 m in surge and the pitch angle is just less than the prescribed  $-20^\circ$ . We also observe a sway deviation from an initial yaw offset.

Examining the remaining 20 seconds of the implemented strategy, we see behavior similar to that presented in Section IV-A, with the exception that the error from the first segment of the trajectory is introduced as the initial condition for the second leg of the concatenated motion. We see the initial negative surge of 0.5 m followed by a positive surge evolution of approximately

0.5 m, as prescribed. The depth evolution shows an overshoot in depth by about 1 m. The pitch evolution after 40 seconds oscillates about zero with a magnitude less than ten degrees. This is a result of not stabilizing the pitch angle to zero before beginning the semi-circle trajectory. Here, the vehicle is simply relying on the righting arm to return it to an upright position. The oscillations present in roll are an artifact of the small distance between the center of gravity and center of buoyancy, i.e., small righting arm. This configuration provides a very controllable vehicle in the sense that it can realize many configurations by use of the on-board thrusts, however this results in a decrease in stability of the AUV. Hence, reduced stability coupled with the open-loop implementation results in the expectation of small perturbations and oscillations in the evolution of the vehicle. The yaw evolution begins with an initial offset that is remedied within the first 10 seconds. Note that this deviation arises during the time that the pitch control is operating. At  $t = 40$  s, we again notice a spike in the yaw, which corresponds to a time when the vehicle is releasing the pitch angle.

## V. CONCLUSIONS

In this paper, we have presented the equations of motion governing the submerged rigid body in both the standard formulation as well as a formulation utilizing the architecture of differential geometry. By use of these geometric equations, we are able to provide solutions to the motion planning problem for AUVs via a geometric reduction. This geometric control theory technique has been proven to be an effective path planning tool for AUVs, especially those operating in an under-actuated condition, see e.g., [10]. Here, we considered a practical application of this path planning technique to examine the bulbous bow of a ship.

Due to the unique shape and location, examination and survey of the bulbous bow provides an interesting motion planning problem for the underwater vehicles. We do not provide an exhaustive survey algorithm, but propose two control strategies which can be used to examine the majority of the bulb. For implementation purposes, the experiments presented here have been scaled down and assume a general form of the bulb. Trajectories to examine an actual bulbous bow of a ship would need to be generated for the specific size and shape of the bulb. The intent here is to present a practical application of an emerging theoretical technique in the area of motion planning for underwater vehicles.

The experimental results presented here extend the work developed in [11], and further validate the design of implementable control strategies by use of differential geometric techniques. This architecture is not just a change of notation for the same equations of motion, but a presentation with a much richer inherent structure. A structure which can be exploited for autonomous path planning in the event of a disabled vehicle (under-actuated) or used to guide the design of future AUVs. Research is currently ongoing to migrate the techniques presented here from the test-bed vehicle ODIN onto an AUV active in the open ocean. The ability to reproduce great implementation results, such as those presented here, gives us a good start to investigate the potential of actual sea trials.

The favorable correlation between theoretical predictions and experimental results presented in this paper are a result of working in a well-known and controlled environment. This will definitely not be the case in the ocean. To move from the pool to the ocean, significant adjustments will be necessary. First off, an AUV cannot operate strictly in an open-loop mode. Poorly known disturbance forces, e.g., ocean currents, are too large and unpredictable to be neglected or accounted for *a priori*, even in a protected harbor or port environment. Applying a purely open-loop control strategy in the ocean, we would expect to see large errors between theoretical predictions and experimental results.

A reasonable approach to begin the migration is to use our control strategies as the desired theoretical predictions, and implement a robust, feedback trajectory-tracking controller that can compensate for the external disturbances. Initial steps in this direction have been taken, and results can be found in [12] and [13]. Once the theory contained in these references becomes well-developed and proven technology, we plan to implement a hybrid control scheme onto ODIN in the pool. We will begin with simple disturbances, such as initial deviations in the state of the vehicle. From the discussion presented in Sections IV-A to IV-C, a known source of error comes from an initial offset in the vehicle's configuration, typically in yaw. Implementing a hybrid controller as previously described will require many upgrades to ODIN, or the use of an alternate AUV for sea trials.

Such extensions present the natural question of applicability of the presented techniques to multiple types of underwater vehicles. First, the theoretical aspect, namely the geometric control, is independent of the choice of the vehicle. The geometric theory is solely based on the fact that the underwater vehicle is an example of a simple mechanical control system; this is true for

any underwater vehicle. Generalizing our work to alternate vehicle designs requires only slight modifications. If the vehicle has three planes of symmetry, which is common for AUVs, the basic foundations and formulations do not change. Obviously, the physical attributes, such as mass, inertia and added mass, need to be altered. This corresponds to the generation of a new kinetic energy metric for the kinematic reduction. Viscous drag coefficients need to be estimated for the specific vehicle, and the locations of the center of buoyancy and center of gravity need to be calculated to appropriately account for the restoration forces and moments. Aside from the obvious physical properties, the only major difference is changing the input control vector fields. These are the basis upon which the decoupling vector fields, and hence the kinematic motions, are determined. This alteration is simply done by expressing the location and output of the actuators of the vehicle in the geometric formulation.

## REFERENCES

- [1] J. Vaganay, M. Elkins, D. Esposito, W. O'Halloran, F. Hover, and M. Kokko, "Ship hull inspection with the HAUV: US Navy and NATO demonstration results," in *Proceedings of the IEEE/MTS Oceans 2006*, 2006.
- [2] GlobalSecurity.org, "USS George H.W. Bush," <http://www.globalsecurity.org/military/systems/ship/bulbous-bow.htm>, 2008, viewed May 2008.
- [3] N. Leonard and P. Krishnaprasad, "Motion control of drift-free, left-invariant systems on lie groups," *IEEE Transactions on Automatic Control*, vol. 40(9), pp. 1539–1554, 1995.
- [4] N. E. Leonard, "Periodic forcing, dynamics and control of underactuated spacecraft and underwater vehicles," in *Proceedings of the 34th IEEE Conference on Decision and Control*, New Orleans, Louisiana, 1995, pp. 3980–3985.
- [5] F. Bullo, N. Leonard, and A. Lewis, "Controllability and motion algorithms for underactuated lagrangian systems on lie groups," *Institute of Electrical and Electronics Engineers. Transactions on Automatic Control*, vol. 45(8), pp. 1437–1454, 2000.
- [6] F. Bullo and K. Lynch, "Kinematic controllability for decoupled trajectory planning in underactuated mechanical systems," *IEEE Transactions. Robotics and Automation*, vol. 17, no. 4, pp. 402–412, 2001.
- [7] F. Bullo, "Trajectory design for mechanical systems: From geometry to algorithms," *European Journal of Control*, vol. 10(5), pp. 397–410, 2004.
- [8] F. Bullo and A. D. Lewis, *Geometric Control of Mechanical Systems*. Springer, 2005.
- [9] M. Chyba and R. N. Smith, "A first extension of geometric control theory to underwater vehicles," in *Proceedings of the 2008 IFAC Workshop on Navigation, Guidance and Control of Underwater Vehicles*, Killaloe, Ireland, 2008, Vol. 2, Part 1.
- [10] R. N. Smith, M. Chyba, G. R. Wilkens, and C. J. Catone, "A geometrical approach to the motion planning problem for a submerged rigid body," *International Journal of Control.*, vol. 82, no. 9, pp. 1641–1656, 2009.
- [11] R. N. Smith, "Geometric control theory and its application to underwater vehicles," Ph.D. dissertation, University of Hawai'i at Manoa, 2008.

- [12] A. Sanyal and M. Chyba, "Robust feedback tracking of autonomous underwater vehicles with disturbance rejection," in *Proceedings of the American Control Conference (ACC)*, St. Louis, MO, 2009.
- [13] S. Singh, A. Sanyal, R. Smith, N. Nordkvist, and M. Chyba, "Robust tracking control of autonomous underwater vehicles in presence of disturbance inputs," in *Proceedings of the 28th International Conference on Offshore Mechanics and Arctic Engineering (OMAE)*, Honolulu, Hawaii, 2009.
- [14] J. Meriam and L. Kraige, *Engineering Mechanics, DYNAMICS*, 4th ed. New York: John Wiley & Sons, Inc., 1997.
- [15] M. D. Ardema, *Newton-Euler Dynamics*. New York: Springer, 2005.
- [16] H. Lamb, *Dynamics*. Cambridge: University Press, 1961.
- [17] T. I. Fossen, *Guidance and Control of Ocean Vehicles*. John Wiley & Sons, 1994.
- [18] SNAME, "Nomenclature for treating the motion of a submerged body through a fluid," The Society of Naval Architects and Marine Engineers, Technical and Research Bulletin No. 1-5, 1950.
- [19] M. do Carmo, *Riemannian Geometry*. Boston: Birkhauser, 1992.
- [20] M. Chyba, T. Haberkorn, R. N. Smith, and S. Choi, "Design and implementation of time efficient trajectories for an underwater vehicle," *Ocean Engineering*, vol. 35, no. 1, pp. 63–76, 2008.
- [21] S. Choi and J. Yuh, "Design of advanced underwater robotic vehicle and graphic workstation," *International Journal of Autonomous Robots*, vol. 3(2/3), pp. 187–194, 1996.
- [22] E. E. Allmendinger, *Submersible Vehicle Design*. SNAME, 1990.
- [23] F. Imlay, "The complete expressions for added mass of a rigid body moving in an ideal fluid," David Taylor Model Basin, Washington D.C., Technical Report DTMB 1528, 1961.
- [24] R. Bhattacharyya, *Dynamics of Marine Vehicles*. John Wiley & Sons, 1978.
- [25] A. Hanai, H. Choi, S. Choi, and J. Yuh, "Minimum energy based fine motion control of underwater robots in the presence of thruster nonlinearity," in *Proceedings of IEEE/RSJ International Conference on Intelligent Robots and Systems*, Las Vegas, Nevada, USA, 2003, pp. 559–564.